Journal of the American Heart Association

ORIGINAL RESEARCH

Early Changes in Rat Heart After High-Dose Irradiation: Implications for Antiarrhythmic Effects of Cardiac Radioablation

Myung-Jin Cha, MD, PhD; Jeong-Wook Seo, MD, PhD; Hak Jae Kim, MD, PhD; Moo-kang Kim, BS; Hye-sun Yoon, BS; Seong Won Jo; Seil Oh, MD, PhD*; Ji Hyun Chang, MD, PhD*

BACKGROUND: Noninvasive cardiac radioablation is employed to treat ventricular arrhythmia. However, myocardial changes leading to early-period antiarrhythmic effects induced by high-dose irradiation are unknown. This study investigated dose-responsive histologic, ultrastructural, and functional changes within 1 month after irradiation in rat heart.

METHODS AND RESULTS: Whole hearts of wild-type Lewis rats (N=95) were irradiated with single fraction 20, 25, 30, 40, or 50 Gy and explanted at 1 day or 1, 2, 3, or 4 weeks' postirradiation. Microscopic pathologic changes of cardiac structures by light microscope with immunohistopathologic staining, ultrastructure by electron microscopy, and functional evaluation by ECG and echocardiography were studied. Despite high-dose irradiation, no myocardial necrosis and apoptosis were observed. Intercalated discs were widened and disrupted, forming uneven and twisted junctions between adjacent myocytes. Diffuse vacuolization peaked at 3 weeks, suggesting irradiation dose-responsiveness, which was correlated with interstitial and intracellular edema. CD68 immunostaining accompanying vacuolization suggested mononuclear cell infiltration. These changes were prominent in working myocardium but not cardiac conduction tissue. Intracardiac conduction represented by PR and QTc intervals on ECG was delayed compared with baseline measurements. ST segment was initially depressed and gradually elevated. Ventricular chamber dimensions and function remained intact without pericardial effusion.

CONCLUSIONS: Mononuclear cell–related intracellular and extracellular edema with diffuse vacuolization and intercalated disc widening were observed within 1 month after high-dose irradiation. ECG indicated intracardiac conduction delay with prominent ST-segment changes. These observations suggest that early antiarrhythmic effects after cardiac radioablation result from conduction disturbances and membrane potential alterations without necrosis.

Key Words: antiarrhythmic effect ■ cardiac radioablation ■ radiation ■ rats ■ ventricular arrhythmia

Noninvasive radioablation, termed stereotactic body radiotherapy or stereotactic ablative radiation therapy in the radiation oncology field, was recently introduced as an alternative noninvasive treatment modality for fatal ventricular arrhythmia.[1,2] The presumed mechanism of antiarrhythmic effect of radioablation was fibrosis, which occurs several months after irradiation and proof-of-principle studies on pulmonary vein isolation demonstrated effective conduction block with radiation-induced fibrosis.[3,4] However, antiarrhythmic effects after radioablation commence at various time points, ranging from immediately postradioablation to 6 months post-treatment.[1,2,5,6] Compared with late response, the cause of early antiarrhythmic effects from radioablation remains unknown, as most studies have focused

Correspondence to: Ji Hyun Chang, MD, PhD, Department of Radiation Oncology, Seoul National University College of Medicine, 101 Daehak-ro, Jongno-gu, Seoul 03080, Korea. E-mail: jh.chang@snu.ac.kr and Seil Oh, MD, PhD, FESC, Department of Internal Medicine, Seoul National University College of Medicine, Seoul National University Hospital, 101 Daehak-ro, Jongno-gu, Seoul 03080, Korea. E-mail: seil@snu.ac.kr

Supplementary Material for this article is available at https://www.ahajournals.org/doi/suppl/10.1161/JAHA.120.019072

*Professor Oh and Professor Chang contributed equally to this work.

For Sources of Funding and Disclosures, see page 11.

JAHA is available at: www.ahajournals.org/journal/jaha

CLINICAL PERSPECTIVE

What Is New?

- In our in vivo study using rat hearts, no myocardial necrosis or apoptosis were observed within 1 month after high-dose irradiation.
- High-dose irradiation resulted in widening of intercalate discs, intracellular cardiac sarcotubular system edema, extracellular swelling, and diffuse mitochondrial damage without definite myofibrillar disruption.
- We demonstrated corresponding ECG changes including intracardiac conduction delay with ST-segment changes.

What Are the Clinical Implications?

- These observations suggest that the early antiarrhythmic effects after cardiac radioablation arise from both cell-to-cell conduction disturbances and cellular membrane instability without direct necrotic damage to myofibril arrangement; this differs from later radiation-induced fibrosis or conventional catheter ablation.
- As early antiarrhythmic effects after radioablation are related to inflammatory changes rather than fibrotic changes, it may be possible to reduce the radiation dose below 25 Gy in single fraction, or to administer fractionated radioablation for medically intractable fatal ventricular tachycardia.

on fibrosis after radioablation in soft tissues. In particular, high-dose radiation effects on cardiomyocytes and surrounding tissues have not been a topic of stereotactic ablative radiation therapy era as the heart is considered a high-risk organ for toxicity.

Pioneering studies in the 1970s to 1980s investigated radiation-induced effects on the heart,[7–10] focusing on cardiac toxicity after radiation therapy. Nevertheless, current clinical needs require the assessment of high-dose irradiation effects at a cellular level at early time points to understand the early antiarrhythmic mechanisms of radiation. In the present in vivo study using rat hearts, we focused on early-period high-dose irradiation effects within 1 month on myocardial components. By observing structural changes in the heart, we expect to understand the mechanism of antiarrhythmic effect that appears early after cardiac radioablation.

METHODS

The data, analytic methods, and study materials will be made available from the corresponding author on reasonable request.

Study Approval

All animal experiments in this study were approved by the Institutional Animal Care and Use Committee of Seoul National University Hospital (approval number: 18-0245-S1A1). Animals were maintained in a facility accredited by the Association for Assessment and Accreditation of Laboratory Animal Care International (#001169) in accordance with the *Guide for the Care and Use of Laboratory Animals, 8th edition*, from the National Resource Council.

Animals

Male 9- to 10-week-old wild-type Lewis rats (OrientBio) (N=95, weighing 300–400 g) were used in this study, including 10 rats in the control group. Different irradiation doses (20, 25, 30, 40, or 50 Gy) were administered. Animals were euthanized for heart explantation on day 1 and weeks 1, 2, 3, and 4, respectively. Electromicroscopic evaluation was performed in the 30-Gy group at various time points for representative, as there was significant difference in histological changes between the 20 Gy/25 Gy group and 30 Gy group in the pilot experiment. Body weight, left ventricular dimensions, echocardiography, and ECG were measured at baseline, at day 1, and at weeks 1, 2, 3, and 4. Three nonirradiated rat hearts were explanted at 1 or 2 weeks as a control group.

Irradiation

Rats were randomly divided into 6 radiation dose groups (a single dose of 0, 20, 25, 30, 40, and 50 Gy, respectively). Rats were anesthetized with Zoletil (tiletamine/zolazepam, 0.04–0.06 mL/kg IM) before irradiation and fixed in a customized acrylic jig. Before irradiation, a computed tomography scan was performed using the Brilliance Big Bore computed tomography simulator (Philips) with 1-mm slice thickness. Computed tomography simulation-based planning was conducted with Eclipse (Varian Medical Systems) to evaluate radiation dosage to the whole heart, lung, and esophagus (Figure S1). Rats were placed in a prone position. Parallel-opposed lateral fields with half-beam blocking were used to cover the whole heart and shield the posterior lungs. A 90% isodose was administered to cover 100% of the heart. Clinac iX (Varian Medical Systems) was used for irradiation. Radiation was delivered at a rate of 6 Gy/min.

Experimentation and Harvesting

Rats were euthanized after irradiation at day 1 and weeks 1, 2, 3, and 4. Rats were anesthetized with Zoletil (tiletamine/zolazepam, 0.04–0.06 mL/kg IM) and maintained with isoflurane (4% for induction; 2–3% for maintenance). Body weight measurement,

ECG, and echocardiography were performed. Blood was replaced with heparinized saline (0.2 units/mL) perfused rapidly from the posterior vena cava. Explanted hearts were fixed for 24 hours in 4% paraformaldehyde solution in 0.1 M phosphate buffer.

Staining

Following dehydration and embedding in paraffin, serial 4-μm sections were cut in the coronal plane showing all 4 chambers and His-bundle area. Sections were stained with hematoxylin and eosin and Masson trichrome for histopathologic evaluation. For immunohistochemical analysis, paraffin blocks were recut and stained with anti-C4d (#MA5-18044), anti-CD3 (#14-0037-82), anti-CD34 (#MA5-18091), anti-CD68 (#MA5-13324), and anti-Des (#MA5-13259) antibodies (Thermo Fisher Scientific). The anti-connexin-43 (Santa Cruz) and anti-α-sarcomeric actin (Sigma) probed with Alexa Fluor 488 (anti-connexin-43)/555 (anti-α-sarcomeric actin) anti-mouse secondary antibody were used for immunofluorescence staining and 4′,6-diamidino-2-phenylindole for nuclear counterstaining. The cells were analyzed using confocal microscopy (LSM710; Zeiss) and Leica Application Suite X software. TUNEL (terminal deoxynucleotidal transferase–mediated biotin–deoxyuridine triphosphate nick-end labeling) assay was conducted to detect cellular apoptosis using a TUNEL kit (#S7101, EMD Millipore Corporation). Slides were scanned using Aperio AT2 (Leica Biosystems) for virtual slides and were analyzed with ImageScope software version 12.4 (Aperio Technologies, Inc.). To evaluate C4d deposition on myocardium, an automated image analysis algorithm Aperio Positive Pixel Count v9 using a default set of parameters was used as previously described.[11] Interpretation of C4d positivity was performed according to 2013 International Society for Heart and Lung Transplantation Working Formulation guidelines.[12]

Electron Microscopy

Tissue specimens from 5 different locations (left/right atrial appendage, left/right ventricular free wall, and interventricular septum) were fixed and processed using JEM-1400 transmission electron microscopy as described by Cocchiaro et al.[13] Standard transmission electron microscopy and immuno-electron microscopy were performed. Digital images of sequential fields were collected for ultrastructural analysis.

ECG and Echocardiography

ECG and echocardiography were performed at baseline preirradiation and on harvest day. ECG rhythm strip was monitored and recorded by Power Lab (AD Instruments). Parameters (heart rate, PR interval, and QRS duration) were measured using LabChart Reader version 8.0 (AD Instruments). The average values of 10 measurements of randomly selected beats during a 1-minute recording were determined. The Bazett formula normalized to average rat RR (QTc(n)-B=QT/(RR/f)(1/2), f=150 ms) was used for QT correction.[14] Echocardiography was performed for cardiac structural and functional evaluation using Toshiba Aplio XG SSA-790A (Toshiba Medical Systems) with a sector probe (Toshiba PST-65AT transducer). Cardiac short-axis M-mode recordings at the mid-left ventricular level were used to obtain ventricular ejection fraction.

Statistical Analysis

Data are presented as mean±SEM. Statistical differences between groups were analyzed by 1-way ANOVA, followed by Tukey multiple comparisons test or Dunnett test. $P<0.05$ was considered statically significant.

RESULTS

High-Dose Irradiation Response: Pathologic Observation

Cardiac myocardium remained intact without rupture or destruction throughout the observation period. The surrounding pericardium was visually normal without effusion. Cardiac valves were intact. No evidence of intracardiac thrombus or coronary artery stenosis was observed. Cardiac myofibrillar arrangement was well preserved with intact Z and M lines on electron microscopy without myofibrillar rupture or discontinuity. To assess myocyte injury after high-dose irradiation, anti-C4d staining and TUNEL assay were performed. No evidence of myocyte necrosis or apoptosis was noted (Figure 1). Nuclear size was not significantly altered.

Intercalated discs were widened, with perturbed cellular connections between adjacent cardiac myocytes (Figure 2). Sporadic focal bulging and multiple gap junction vesicles of variable sizes were noted close to damaged intercalated discs. Longitudinal continuity of intercalated discs was maintained. At week 4, intercalated disc lining was twisted and thickened relative to baseline on both atrial and ventricular sides. The incidence did not vary according to timing of observation or location. In the immunofluorescence staining of connexin-43, we observed a decreased expression of connexin-43 at 2 or 3 weeks, but slightly increased at 4 weeks (Figure S2).

Diffuse vacuolization and loosened myocardial architecture were noted (Figure 3). Vacuolization observed in hematoxylin and eosin staining comprised interstitial

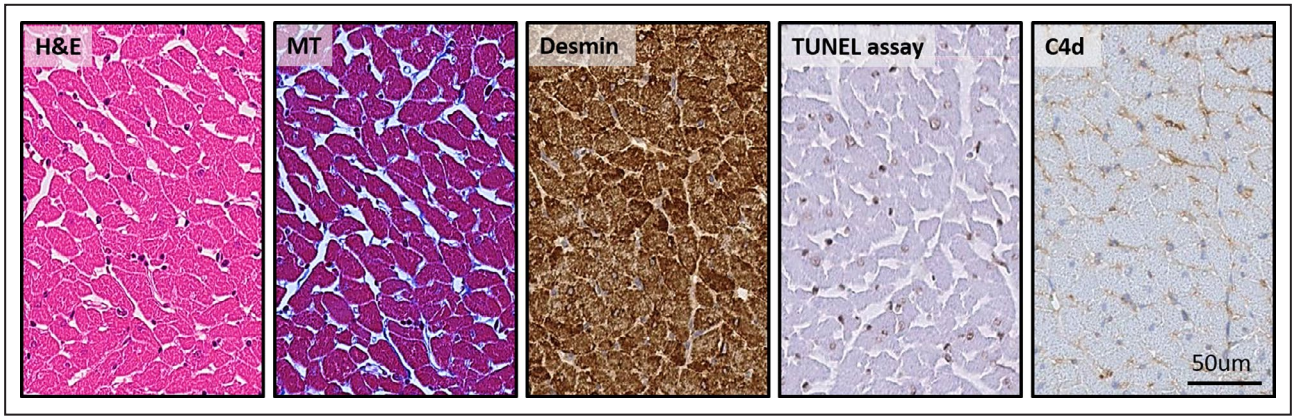

Figure 1. Ventricular myocardium irradiated with 30 Gy at 4 weeks.
Irradiated left ventricular free wall subendocardium of rats was stained with hematoxylin and eosin (H&E), Masson trichrome (MT), and immunohistochemistry (Desmin, TUNEL [terminal deoxynucleotidal transferase–mediated biotin–deoxyuridine triphosphate nick-end labeling] assay, and C4d immunostaining). Myocyte necrosis and apoptosis were not observed in rat hearts irradiated by 20 to 50 Gy. Intercellular space (interstitium) was widened but not fibrotic. Cellular rupture and destruction of myocytes were not observed. (×400 Magnification.)

edema and intracellular swelling on transmission electron microscopy (Figure 4). These effects were dose-dependent, peaked at 3 weeks, and were reversed at 4 weeks. The vacuolization area per high-power field increased with radiation dose. Immunohistochemical staining revealed CD68 immunopositivity in the interstitial area corresponding to regions of vacuolization, indicating macrophage/mononuclear interstitial infiltration into interstitial vacuoles. C4d immunopositivity on vacuolization was less prominent in the His-bundle area than in atrial or ventricular myocardial areas (Figure S3).

Capillary diameter was markedly dilated after week 2, potentially leading to microvascular extravasation and resultant interstitial swelling. Anti-CD34 immunostaining of capillaries did not reveal alterations in capillary number or evidence of capillary apoptosis based on TUNEL assay (Figure S4). Red blood cells were attached to capillary vessel walls. Neutrophil infiltration was scarce. Intracellular structural damage including cytoplasmic swelling and mitochondrial damage contributed to intracellular vacuolization (Figure S5). Cytoplasmic swelling was accompanied with sarcomere and sarcoplasmic reticular swelling, resulting in increased intermyofibrillar space with intracellular reticular pattern of individual myocytes. Intracellular mitochondrial damage included mitochondrial rupture, fission, or fusion. Mitophagy was noted, indicating mitophagosis of damaged mitochondria. This change was prominent from week 2 and was partially resolved at week 4.

Myocardial endocardial and epicardial lining was thickened with prominent hyperplasia and interstitial edema (Figure S6). Intracardiac coronary arteries and arterioles exhibited intimal proliferation and perivascular edema beginning from 20 Gy/2 weeks in a dose- and time-dependent manner (Figure S7). Fibroblast and inflammatory cell recruitment were

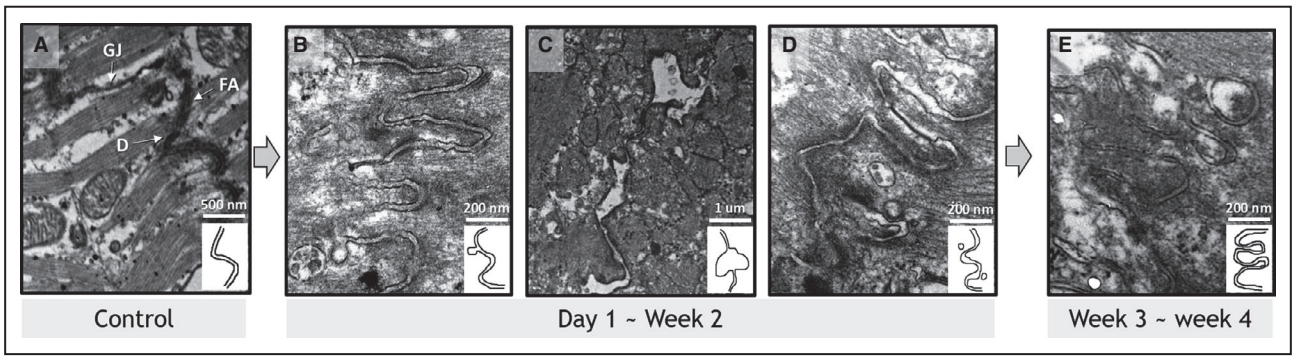

Figure 2. Electron microscope examination of the left ventricular myocardium of irradiated rat heart (30 Gy single fraction).
Compared with normal intercalated discs (**A**), irradiated intercalated discs exhibited irregular widening focal protrusion (**B**) or segmental separation (**C**) peaking at 1 week. These abnormalities were observed in 30 Gy-irradiated rats harvested at day 1 and were rarely observed after week 2. From week 2, intercalated discs exhibited irregularly widened longitudinal cell connections with adjacent gap junction vesicles (**D**). Damaged intercalated discs were narrowed after 3 weeks. Remodeling was uneven and twisted (**E**). (×50 000 Magnification.)

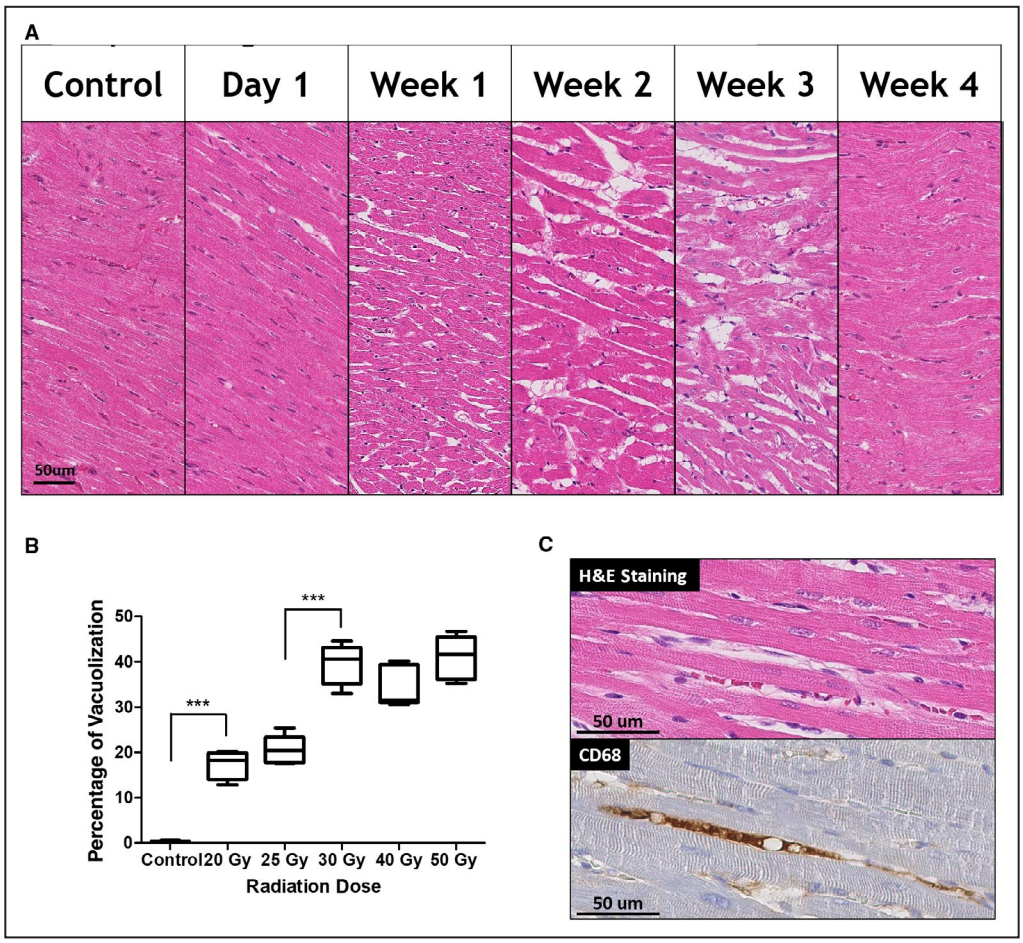

Figure 3. Interstitial vacuolization.
A, Temporal changes of the left ventricular subendocardial vacuolization. (×400 Magnification.) **B**, Boxplot of the percentage of vacuolization at 3 weeks according to radiation dose. The extent of vacuolization in 5 high-power field was measured at left ventricular subendocardium using an Aperio Imagescope (Leica). All groups were statistically different from each group, except the 20 and 25 Gy groups and the 30, 40, 50 Gy groups. *** indicates $P<0.001$. **C**, The vacuolized area on hematoxylin and eosin (H&E) staining showed positive staining for CD68. (×400 Magnification.) Statistical difference was determined by 1-way ANOVA with Tukey post hoc analysis.

noted between loosened externa. No obvious histopathologic damage was noted in cardiac valvular structures and pericardium. The main observations are depicted in Figure 5.

ECG Results

Resting heart rate was increased after irradiation. The PR interval, representing the conduction velocity from atrium to ventricle, was slightly delayed after 2 weeks. The corrected QT interval, representing intraventricular conduction properties, was prolonged relative to baseline. The ST segment was depressed after irradiation but significantly elevated after 2 weeks in most cases. No clinically significant abnormal tachyarrhythmias or bradyarrhythmias were noted in all dose groups. Occasional atrial premature beats were observed in rats irradiated with 40 Gy or 50 Gy at 2 to 4 weeks, which were absent in lower-dose groups. Detailed ECG parameters (heart rate, PR interval, and QTc interval) and ST-segment changes after irradiation are presented in Figure 6.

Echocardiography Results

No significant effects of irradiation on left ventricular ejection fraction were observed (Figure S8). No pericardial effusion or intracardiac thrombi were observed. Left ventricular chamber size and wall thickness were within the normal range. Cardiac valvular motion was visually normal.

Body Weight and Laboratory Test Results

Body weights decreased during follow-up after irradiation, especially in the 40- and 50 Gy groups after 3 weeks. White blood cell counts were decreased at

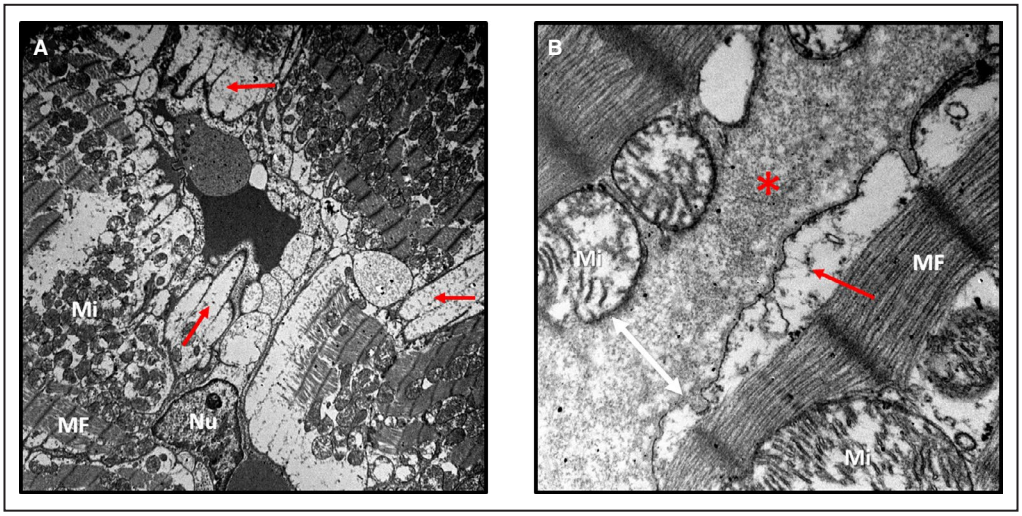

Figure 4. Interstitial and cytoplasmic edema after irradiation.
A, Rat left ventricular midmyocardium on electron microscopy (×5000 magnification). **B**, Rat left ventricular midmyocardium on electron microscopy (×40 000 magnification), left ventricle irradiated with 30 Gy (3 weeks). Cellular membranes were dilated because of cytoplasmic swelling (red arrows). Interstitial edema widened intercellular spaces (red asterisks and white arrow). Subsarcolemmal and interfibrillar mitochondria (marked as "Mi") were damaged and variable in size. Myofibrils (MFs) with Z and M lines were intact. No remarkable abnormalities in myocyte nuclei (marked as "Nu") were noted.

1 week but subsequently normalized. Neutrophil proportion was slightly increased after irradiation. Body weights and laboratory data are presented in Figure S9.

DISCUSSION

In this study, we assessed the effects of high-dose irradiation of rat heart. High-dose irradiation resulted in widening of intercalated discs, intracellular cardiac sarcotubular system edema, extracellular swelling, and diffuse mitochondrial damage without definite myofibrillar disruption. We demonstrated corresponding ECG changes including intracardiac conduction delay with ST-segment changes. With regard to cardiac arrhythmias, the present study is the first to suggest that cell-to-cell conduction disturbances and cellular membrane potential alterations result in early electrophysiological changes after cardiac radioablation.

Most preclinical and clinical studies on cardiac effects after irradiation have examined radiation-induced heart disease based on autopsy findings of myocardial fibrosis after massive radiotherapy in humans.[15] Although pioneering research included early cardiac responses after, the clinical importance of early changes was less significant than that of late changes, as they were not prominent in light microscopy and ultrastructural changes were largely reversible.[8–10,16] Most early studies used doses of 10 to 20 Gy. Recently, Kiscsatari et al[17] performed an in vivo study in rat hearts using the same doses as those in our study. However, their study focused on radiation toxicity in the heart, and tissue was harvested at week 19. They reported that fibrosis was present in groups irradiated with ≥40 Gy at 19 weeks after irradiation.

Based on prior preclinical studies demonstrating radiation-induced cardiac fibrosis, there have been several attempts to test the feasibility of radiotherapy for arrhythmias, mainly targeting pulmonary vein isolation for atrial fibrillation.[4,18–21] Sharma et al[20] described pathologic changes in targets at the cavotricuspid isthmus, atrioventricular node, pulmonary vein–left atrial junction, and left atrial appendage of mini-swine on 25 to 196 days after radiation. Further, the authors reported discrete fibrosis with elongated fibroblasts, which was not observed in the early phase after radiation. Rapp et al[4] reported pathological changes in cardiomyocytes in a swine model, revealing vascular damage, fibrosis, and vacuolization after 6 months of C-ion radiation. Several preclinical studies have been performed to test the feasibility of radiotherapy for pulmonary vein isolation.[18,19,22] To interpret irradiation-induced conduction block, pathologic findings in prior studies have focused on obvious differences between irradiated areas including fibrosis and undamaged nonirradiated areas.[18–21] These preclinical studies have helped to determine the therapeutic radiation dose for arrhythmias, as the results demonstrated that electrophysiological changes or fibrotic scarring were achievable at doses above 25 Gy after several weeks to months postirradiation.

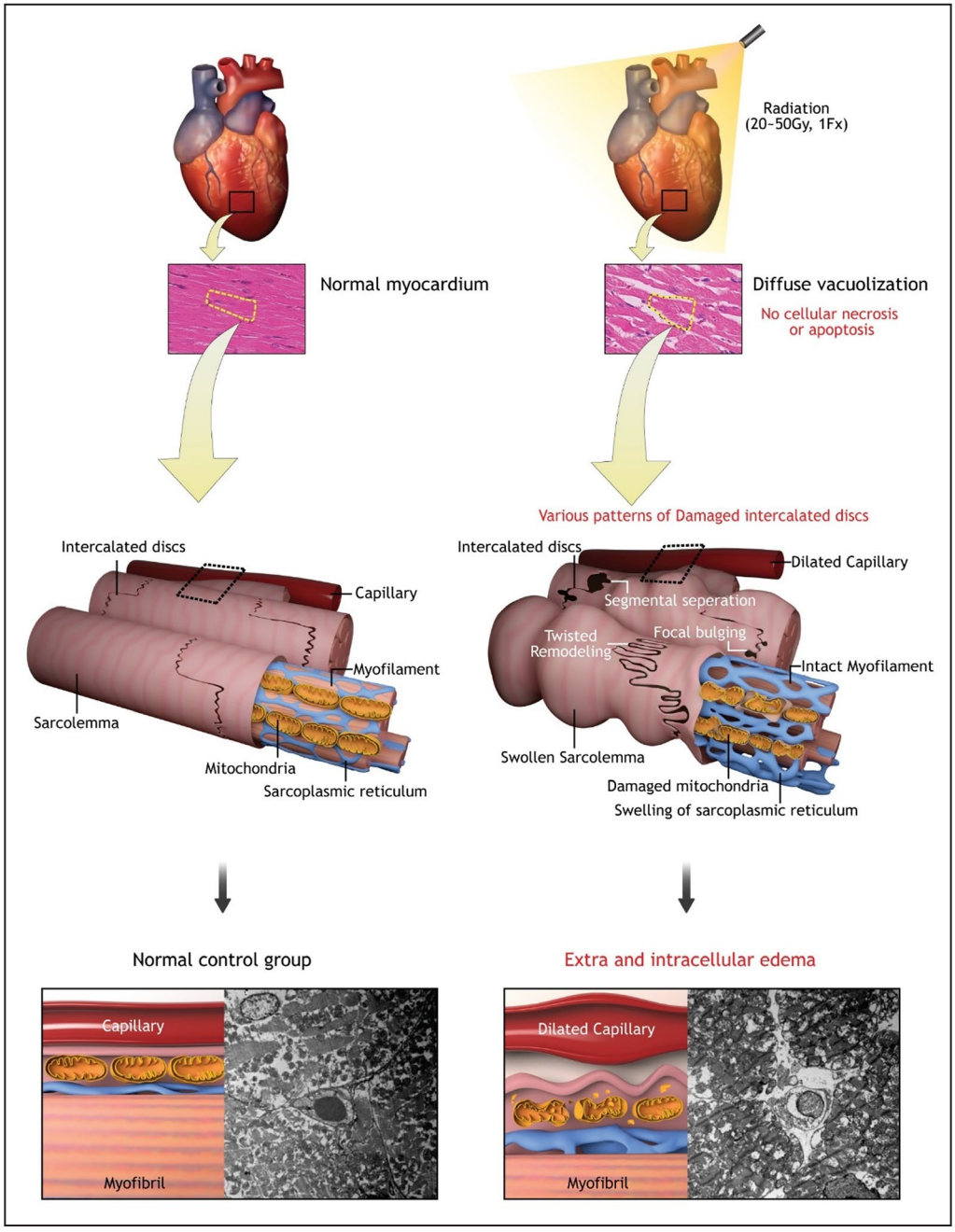

Figure 5. Main histopathologic findings.
Irradiated rat heart myocardium (right) and normal rat heart myocardium (left) were compared. No cellular necrosis or apoptosis after irradiation was noted. Diffuse vacuolization was correlated with interstitial and subsarcolemmal edema. Intercalated discs between myocytes were widened with diverse patterns.

Conversely, other reports demonstrated complete scarring at higher doses.[19,21,22] Although these preclinical studies focused on atrial fibrillation, anticipated antiarrhythmic mechanisms after radioablation for ventricular tachycardia included fibrosis in the context of arrhythmia treatment.

In general, radiation-induced fibrosis occurs several months after radiotherapy.[23] However, real-world data have demonstrated antiarrhythmic effects as early as immediately after radioablation.[2,6,24] Thus, the present study was conducted to elucidate the mechanisms underpinning these effects. We did not observe necrosis or apoptosis in myocardium, which differs from the results of conventional catheter ablation techniques using radiofrequency and cryoenergy. Radiofrequency catheter ablation immediately generates permanent tissue necrosis by direct resistive heating and indirect passive conductive heating.[25]

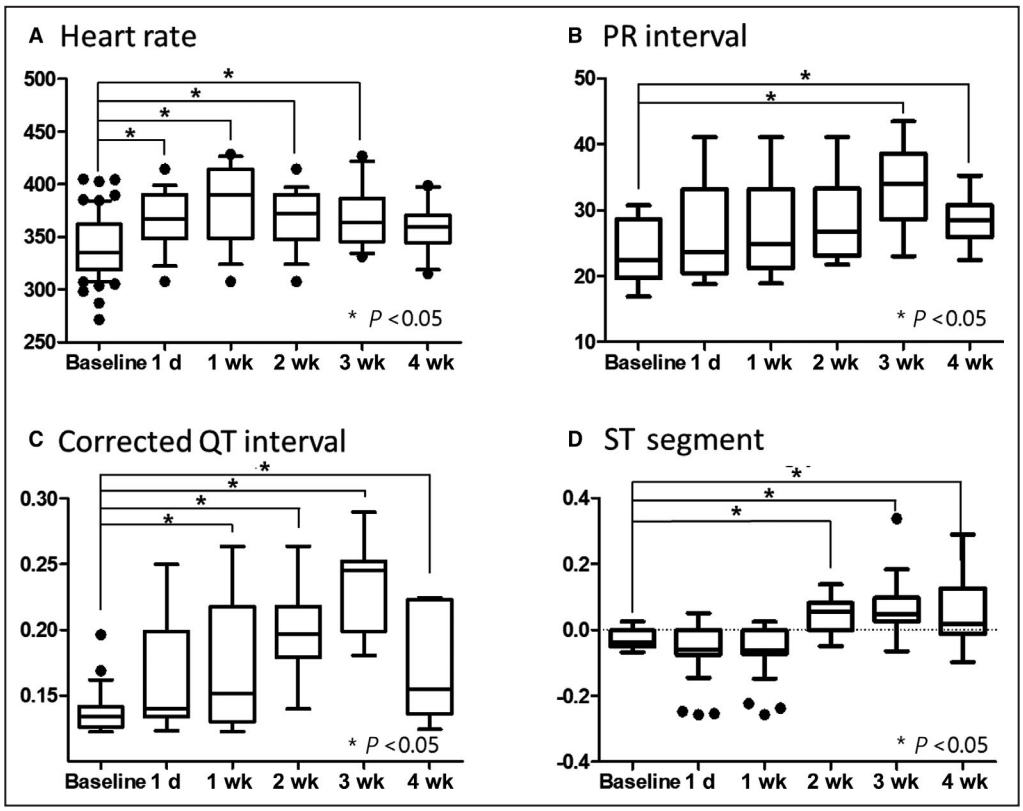

Figure 6. ECG changes.
Average values of 10 measurements of randomly selected beats during a 1-minute recording were determined. The sample size was 15 per group at each time point. **A**, Resting heart rate was increased after irradiation compared with baseline measurements. **B**, The PR interval, representing the conduction velocity from atrium to ventricle, was slightly delayed and peaked at 3 weeks. **C**, The corrected QT interval, representing the intraventricular conduction property, was prolonged relative to baseline. **D**, The ST segment was depressed after irradiation but elevated after 2 weeks in most cases. The statistical difference between groups was calculated using 1-way ANOVA with Dunnett post hoc analysis.

Several factors influence optimal lesion formation, including conductive cooling by surrounding blood flow, size of ablation catheter tip, location of targeted substrate, and catheter manipulation techniques, which pose limitations for radiofrequency catheter ablation.[26] With regards to cryoablation, myocardial cell freezing causes rupture and cell necrosis, eventually leading to apoptosis. Extracellular ice crystal formation contributes to mechanical cell damage causing injury to cell organelles and membranes, which results in intracellular hyperosmotic stress, volume loss, and injury to cell constituents.[27] As reported here, the early effects after cardiac radioablation are underpinned by distinct mechanisms unrelated to cellular necrosis. The cardiac radioablation dose of 25 Gy used in the clinical setting for ventricular tachycardia results in immediate responses. The current study applied higher doses up to 50 Gy, but no evidence of cardiomyocyte apoptosis or necrosis was noted.[2,28]

Intercalated disc widening, intracellular cardiac sarcotubular system edema, and extracellular swelling observed on electron microscopy are distinct radiation-induced features largely consistent with previous findings reported in the 1970 to 1980s. Khan[9] reported dissociation of intercalated discs observed 24 and 48 hours postirradiation with 10 Gy and 13 Gy. Similarly, Cillers et al[10] investigated the effects of irradiation on rat heart and reported intercalated disc damage as early as 6 hours postirradiation, which peaked at 3 weeks; these changes receded 60 days after irradiation with 20 Gy. A major component of intercalated discs are gap junction channels responsible for electrical cell-to-cell propagation and arrhythmogenesis in cardiac cells.[29] Although we did not employ an arrhythmia model, we speculate that intercalated disc widening may alter electrophysiological characteristics, based on previous reports on the relationship between intercalated disc remodeling and arrhythmogenesis.[30,31]

Another notable finding regarding cardiac conduction disturbances was myocardial inflammatory responses to irradiation as suggested by prominent intracellular and extracellular swelling including

sarcotubular systemic dilatation. Capillary dilation and red blood cell attachment to vessel walls strongly suggested an inflammatory process. Extravasated fluid from capillaries may have induced interstitial and intracellular edema, manifesting as prominent edematous sarcolemma and dilatated sarcoplasmic reticulum. Neutrophil infiltration and aggregation were not observed, but sporadic mononuclear cell infiltration was observed with anti-CD68 staining within interstitial swollen areas. These observations can be summarized as microvascular inflammatory responses to irradiation. After the early phase, changes would proceed to irreversible fibrosis within several months as described by previous reports.[17,32] We did not observe changes in conduction tissue even though we employed higher doses (up to 50 Gy) than those used in previous studies on radiation toxicity on the heart, which used doses around 20 Gy. Viczenczova et al[33–35] showed that a single dose of 25 Gy irradiation resulted in compensatory upregulated myocardial connexin-43, which could not be confirmed by our finding. We could tell that the connexin-43 expression was disorganized after irradiation. The difference could possibly be the result of the observation period, as the studies from Viczenczova et al were 6 weeks after irradiation and 1 day to 4 weeks in the current study. Further research is needed on the mechanism of connexin-43 expression changes.

Mitochondrial damage after irradiation has been proposed to underpin radiation-induced heart disease.[36–38] Several mechanisms including oxidative stress, transcription factor pathways such as glutathione S-transferase alpha 4/Nrf2 or peroxisome proliferator–activated receptor-α, and apoptosis have been proposed to underscore mitochondrial damage related to radiation-induced heart disease, but these remain under investigation.

No clinically significant tachyarrhythmias or conduction block were observed; however, ECG changes suggested that high-dose irradiation affected cardiac electrophysiological properties. Although heart rate was significantly increased after irradiation, intracardiac conduction velocity was delayed. ST-segment elevation following depression was notable and is commonly observed in various cardiac diseases such as myocarditis, ischemic heart disease, or stress-induced cardiomyopathy.[39] Based on our results, it can be speculated that cell-to-cell conduction disturbances and membrane potential alterations caused by inflammatory processes result in ECG changes. From these pathologic and ECG findings, early electrophysiological changes leading to antiarrhythmic effects arise from modifications in electrical characteristics of cardiac tissue driven by altered conduction properties rather than necrosis or apoptosis. Therefore, early antiarrhythmic effects after radioablation differ from late-phase antiarrhythmic effects. Multiple ionic currents, transporters, signaling pathways, and their interaction in ventricular myocytes underpin the clinical manifestation of ventricular tachycardia.[40] Our results suggest that early antiarrhythmic effects after radioablation are related to inflammatory changes rather than fibrotic changes. Further, the radiation dose could be reduced <25 Gy in single fraction, or fractionated radioablation could be administered for medically intractable fatal ventricular tachycardia storm.

Our study has several limitations. First, experiments were performed in healthy rats. Although research using animal models with ventricular tachycardia is the most desirable, it is challenging to produce homogeneous ventricular tachycardia in all subjects. Therefore, we performed experiments in normal heart tissue with a large number of study subjects and employed cardiac conditions that were as homogenous as possible. Second, cardiac electrophysiologic properties differ between rats and humans. Our study revealed irradiation effects on normal rat heart, which may not directly reflect antiarrhythmic effects on human ventricular tachycardia. Third, our data presented histopathological findings relating ECG changes to antiarrhythmic effects, but detailed electrophysiologic mechanisms of membrane potential alterations or cell-to-cell conduction disturbances could not be determined from histopathological observations. Further studies assessing cellular action potential and myocardial electrical propagation changes, as well as proteomics analysis constituting membrane ionic channels should be performed in the future.

CONCLUSIONS

Intercalated disc widening, diffuse interstitial vacuolization, and subsarcolemmal swelling with mitochondrial damage were prominent observations within 1 month after high-dose irradiation. These structural changes may be correlated with cardiac conduction property changes, resulting in intracardiac conduction velocity delay in ECG findings. These observations suggest that early antiarrhythmic effects after cardiac radioablation arise from both cell-to-cell conduction disturbances and cellular membrane instability without direct necrotic damage to myofibril arrangement, which differs from later radiation fibrosis or conventional catheter ablation.

ARTICLE INFORMATION

Received October 19, 2020; accepted January 14, 2021.

Affiliations

From the Division of Cardiology, Department of Internal Medicine (M.C., M.K., H.Y., S.O.) and Departments of Pathology (J.S.), Seoul National University Hospital, Seoul, South Korea; Department of Radiation Oncology, Seoul

National University College of Medicine, Seoul, Korea (H.J.K., J.H.C.); Department of Radiation Oncology, Seoul National University Hospital, Seoul, South Korea (H.J.K., J.H.C.); Cancer Research Institute, Seoul National University College of Medicine, Seoul, Korea (H.J.K.); and Seoul National University College of Medicine, Seoul, Korea (S.W.J.).

Sources of Funding

This research was supported by the National Research Foundation of Korea (NRF) funded by the Ministry of Science & Information Communication Technology (NRF-2018M2A2B3A01070410 and NRF-2020R1A2C1013832).

Disclosures

None.

Supplementary Material

Figures S1–S9

REFERENCES

1. Kavanaugh JA, Holler S, DeWees TA, Robinson CG, Bradley JD, Iyengar P, Higgins KA, Mutic S, Olsen LA. Multi-institutional validation of a knowledge-based planning model for patients enrolled in RTOG 0617: implications for plan quality controls in cooperative group trials. *Pract Radiat Oncol*. 2019;9:e218–e227.DOI: 10.1016/j.prro.2018.11.007.
2. Cuculich PS, Schill MR, Kashani R, Mutic S, Lang A, Cooper D, Faddis M, Gleva M, Noheria A, Smith TW, et al. Noninvasive cardiac radiation for ablation of ventricular tachycardia. *N Engl J Med*. 2017;377:2325–2336.DOI: 10.1056/NEJMoa1613773.
3. Ipsen S, Blanck O, Oborn B, Bode F, Liney G, Hunold P, Rades D, Schweikard A, Keall PJ. Radiotherapy beyond cancer: target localization in real-time MRI and treatment planning for cardiac radiosurgery. *Med Phys*. 2014;41:120702. DOI: 10.1118/1.4901414.
4. Rapp F, Simoniello P, Wiedemann J, Bahrami K, Grünebaum V, Ktitareva S, Durante M, Lugenbiel P, Thomas D, Lehmann HI, et al. Biological cardiac tissue effects of high-energy heavy ions – investigation for myocardial ablation. *Sci Rep*. 2019;9:5000. DOI: 10.1038/s41598-019-41314-x.
5. Neuwirth R, Cvek J, Knybel L, Jiravsky O, Molenda L, Kodaj M, Fiala M, Peichl P, Feltl D, Januška J, et al. Stereotactic radiosurgery for ablation of ventricular tachycardia. *Europace*. 2019;21:1088–1095.DOI: 10.1093/europace/euz133.
6. Jumeau R, Ozsahin M, Schwitter J, Vallet V, Duclos F, Zeverino M, Moeckli R, Pruvot E, Bourhis J. Rescue procedure for an electrical storm using robotic non-invasive cardiac radio-ablation. *Radiother Oncol*. 2018;128:189–191.DOI: 10.1016/j.radonc.2018.04.025.
7. Fajardo LF, Stewart JR. Capillary injury preceding radiation-induced myocardial fibrosis. *Radiology*. 1971;101:429–433.DOI: 10.1148/101.2.429.
8. Fajardo LF, Stewart JR. Pathogenesis of radiation-induced myocardial fibrosis. *Lab Invest*. 1973;29:244–257.
9. Khan MY. Radiation-induced cardiomyopathy. I. An electron microscopic study of cardiac muscle cells. *Am J Pathol*. 1973;73:131–146.
10. Cilliers GD, Harper IS, Lochner A. Radiation-induced changes in the ultrastructure and mechanical function of the rat heart. *Radiother Oncol*. 1989;16:311–326.DOI: 10.1016/0167-8140(89)90044-3.
11. Brazdziute E, Laurinavicius A. Digital pathology evaluation of complement C4d component deposition in the kidney allograft biopsies is a useful tool to improve reproducibility of the scoring. *Diagn Pathol*. 2011;6:S5. DOI: 10.1186/1746-1596-6-S1-S5.
12. Berry GJ, Burke MM, Andersen C, Bruneval P, Fedrigo M, Fishbein MC, Goddard M, Hammond EH, Leone O, Marboe C, et al. The 2013 international society for heart and lung transplantation working formulation for the standardization of nomenclature in the pathologic diagnosis of antibody-mediated rejection in heart transplantation. *J Heart Lung Transplant*. 2013;32:1147–1162.DOI: 10.1016/j.healun.2013.08.011.
13. Boerma M, Zurcher C, Esveldt I, Schutte-Bart CI, Wondergem J. Histopathology of ventricles, coronary arteries and mast cell accumulation in transverse and longitudinal sections of the rat heart after irradiation. *Oncol Rep*. 2004;12:213–219.DOI: 10.3892/or.12.2.213.
14. Kmecova J, Klimas J. Heart rate correction of the QT duration in rats. *Eur J Pharmacol*. 2010;641:187–192.DOI: 10.1016/j.ejphar.2010.05.038.
15. Rubin E, Camara J, Grayzel DM, Zak FG. Radiation-induced cardiac fibrosis. *Am J Med*. 1963;34:71–75.DOI: 10.1016/0002-9343(63)90039-1.
16. Stewart JR, Fajardo LF, Gillette SM, Constine LS. Radiation injury to the heart. *Int J Radiat Oncol Biol Phys*. 1995;31:1205–1211.DOI: 10.1016/0360-3016(94)00656-6.
17. Kiscsatari L, Sarkozy M, Kovari B, Varga Z, Gomori K, Morvay N, Lepran I, Hegyesi H, Fabian G, Cserni B, et al. High-dose radiation induced heart damage in a rat model. *Vivo*. 2016;30:623–631.
18. Bode F, Blanck O, Gebhard M, Hunold P, Grossherr M, Brandt S, Vonthein R, Thiele H, Dunst J, Rades D. Pulmonary vein isolation by radiosurgery: implications for non-invasive treatment of atrial fibrillation. *Europace*. 2015;17:1868–1874.DOI: 10.1093/europace/euu406.
19. Blanck O, Bode F, Gebhard M, Hunold P, Brandt S, Bruder R, Grossherr M, Vonthein R, Rades D, Dunst J. Dose-escalation study for cardiac radiosurgery in a porcine model. *Int J Radiat Oncol Biol Phys*. 2014;89:590–598.DOI: 10.1016/j.ijrobp.2014.02.036.
20. Sharma A, Wong D, Weidlich G, Fogarty T, Jack A, Sumanaweera T, Maguire P. Noninvasive stereotactic radiosurgery (CyberHeart) for creation of ablation lesions in the atrium. *Heart Rhythm*. 2010;7:802–810. DOI: 10.1016/j.hrthm.2010.02.010.
21. Refaat MM, Ballout JA, Zakka P, Hotait M, Al Feghali KA, Gheida IA, Saade C, Hourani M, Geara F, Tabbal M, et al. Swine atrioventricular node ablation using stereotactic radiosurgery: methods and in vivo feasibility investigation for catheter-free ablation of cardiac arrhythmias. *J Am Heart Assoc*. 2017;6:e007193. DOI: 10.1161/JAHA.117.007193.
22. Zei PC, Wong D, Gardner E, Fogarty T, Maguire P. Safety and efficacy of stereotactic radioablation targeting pulmonary vein tissues in an experimental model. *Heart Rhythm*. 2018;15:1420–1427.DOI: 10.1016/j.hrthm.2018.04.015.
23. Straub JM, New J, Hamilton CD, Lominska C, Shnayder Y, Thomas SM. Radiation-induced fibrosis: mechanisms and implications for therapy. *J Cancer Res Clin Oncol*. 2015;141:1985–1994.DOI: 10.1007/s00432-015-1974-6.
24. Loo BW, Soltys SG, Wang L, Lo A, Fahimian BP, Iagaru A, Norton L, Shan X, Gardner E, Fogarty T, et al. Stereotactic ablative radiotherapy for the treatment of refractory cardiac ventricular arrhythmia. *Circ Arrhythm Electrophysiol*. 2015;8:748–750.DOI: 10.1161/CIRCEP.115.002765.
25. Nath S, Lynch C III, Whayne JG, Haines DE. Cellular electrophysiological effects of hyperthermia on isolated guinea pig papillary muscle. *Implications for catheter ablation. Circulation*. 1993;88:1826–1831.DOI: 10.1161/01.CIR.88.4.1826.
26. Nath S, DiMarco JP, Haines DE. Basic aspects of radiofrequency catheter ablation. *J Cardiovasc Electrophysiol*. 1994;5:863–876.DOI: 10.1111/j.1540-8167.1994.tb01125.x.
27. Mazur P. Cryobiology: the freezing of biological systems. *Science*. 1970;168:939–949.DOI: 10.1126/science.168.3934.939.
28. Robinson CG, Samson PP, Moore KMS, Hugo GD, Knutson N, Mutic S, Goddu SM, Lang A, Cooper DH, Faddis M, et al. Phase I/II trial of electrophysiology-guided noninvasive cardiac radioablation for ventricular tachycardia. *Circulation*. 2019;139:313–321.DOI: 10.1161/CIRCULATIONAHA.118.038261.
29. Kleber AG, Saffitz JE. Role of the intercalated disc in cardiac propagation and arrhythmogenesis. *Front Physiol*. 2014;5:404.
30. Kontaridis MI, Geladari EV, Geladari CV. Structural alterations in the hypertensive heart disease result in intercalated disc remodeling and arrhythmias. *Hypertension and cardiovascular disease*. Cham: Springer; 2016;97–120. DOI: 10.1007/978-3-319-39599-9_8.
31. Rizzo S, Lodder EM, Verkerk AO, Wolswinkel R, Beekman L, Pilichou K, Basso C, Remme CA, Thiene G, Bezzina CR. Intercalated disc abnormalities, reduced na(+) current density, and conduction slowing in desmoglein-2 mutant mice prior to cardiomyopathic changes. *Cardiovasc Res*. 2012;95:409–418.DOI: 10.1093/cvr/cvs219.
32. Heidenreich PA, Kapoor JR. Radiation induced heart disease: systemic disorders in heart disease. *Heart*. 2009;95:252–258.
33. Viczenczova C, Kura B, Egan Benova T, Yin C, Kukreja RC, Slezak J, Tribulova N, Szeiffova BB. Irradiation-induced cardiac connexin-43 and miR-21 responses are hampered by treatment with atorvastatin and aspirin. *Int J Mol Sci*. 2018;19:1128. DOI: 10.3390/ijms19041128.
34. Viczenczova C, Kura B, Chaudagar KK, Szeiffova Bacova B, Egan Benova T, Barancik M, Knezl V, Ravingerova T, Tribulova N, Slezak J. Myocardial connexin-43 is upregulated in response to acute cardiac injury in rats. *Can J Physiol Pharmacol*. 2017;95:911–919.DOI: 10.1139/cjpp-2016-0680.

35. Viczenczova C, Szeiffova Bacova B, Egan Benova T, Kura B, Yin C, Weismann P, Kukreja R, Slezak J, Tribulova N. Myocardial connexin-43 and PKC signalling are involved in adaptation of the heart to irradiation-induced injury: implication of miR-1 and miR-21. *Gen Physiol Biophys*. 2016;35:215–222. DOI: 10.4149/gpb_2015038.
36. Livingston K, Schlaak RA, Puckett LL, Bergom C. The role of mitochondrial dysfunction in radiation-induced heart disease: from bench to bedside. *Front Cardiovasc Med*. 2020;7:20. DOI: 10.3389/fcvm.2020.00020.
37. Kam WW, Banati RB. Effects of ionizing radiation on mitochondria. *Free Radic Biol Med*. 2013;65:607–619.DOI: 10.1016/j.freeradbiomed.2013.07.024.
38. Wang H, Wei J, Zheng Q, Meng L, Xin Y, Yin X, Jiang X. Radiation-induced heart disease: a review of classification, mechanism and prevention. *Int J Biol Sci*. 2019;15:2128–2138.DOI: 10.7150/ijbs.35460.
39. Testani JM, Kolansky DM, Litt H, Gerstenfeld EP. Focal myocarditis mimicking acute ST-elevation myocardial infarction: diagnosis using cardiac magnetic resonance imaging. *Tex Heart Inst J*. 2006;33:256–259.
40. Qu Z, Weiss JN. Mechanisms of ventricular arrhythmias: from molecular fluctuations to electrical turbulence. *Annu Rev Physiol*. 2015;77:29–55. DOI: 10.1146/annurev-physiol-021014-071622.

SUPPLEMENTAL MATERIAL

Figure S1. Treatment plan based on computed Tomography (CT) simulation.

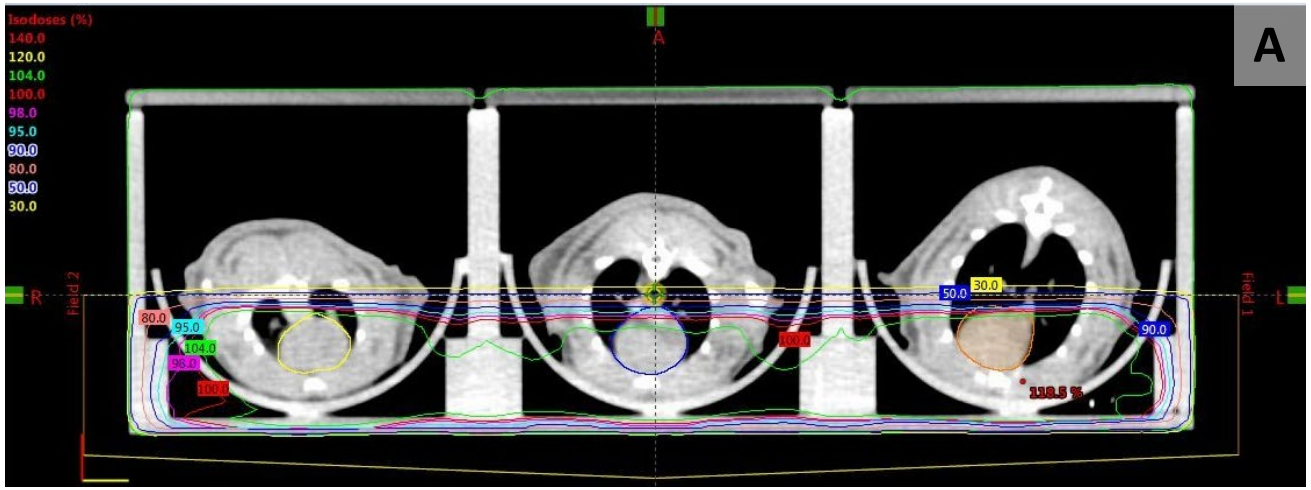

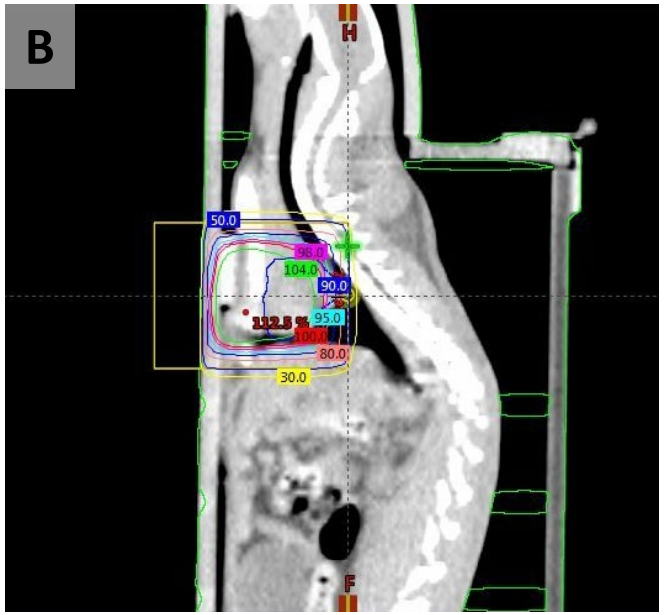

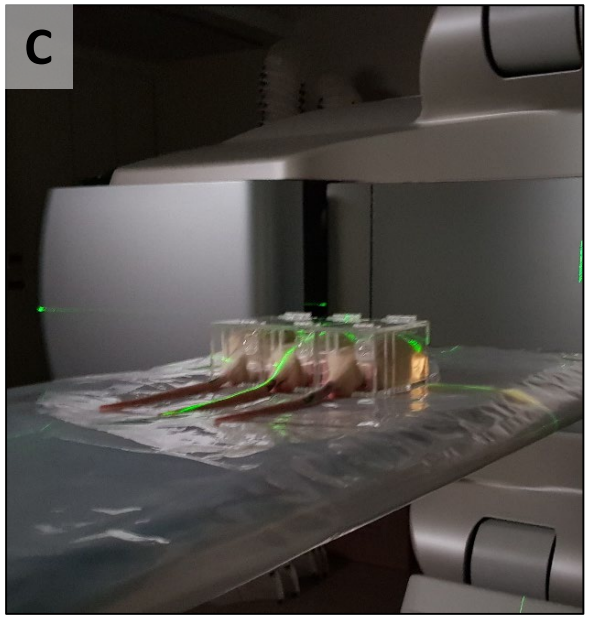

Simulation CT was taken under prone position for the planning. Hearts in each rat were delineated. Parallel beams with half beam block principles were used. (A) Dose distributions in axial and (B) sagittal view. (C) Customized jig was used for immobilization.

Figure S2. Immunofluorescence staining of connexin-43.

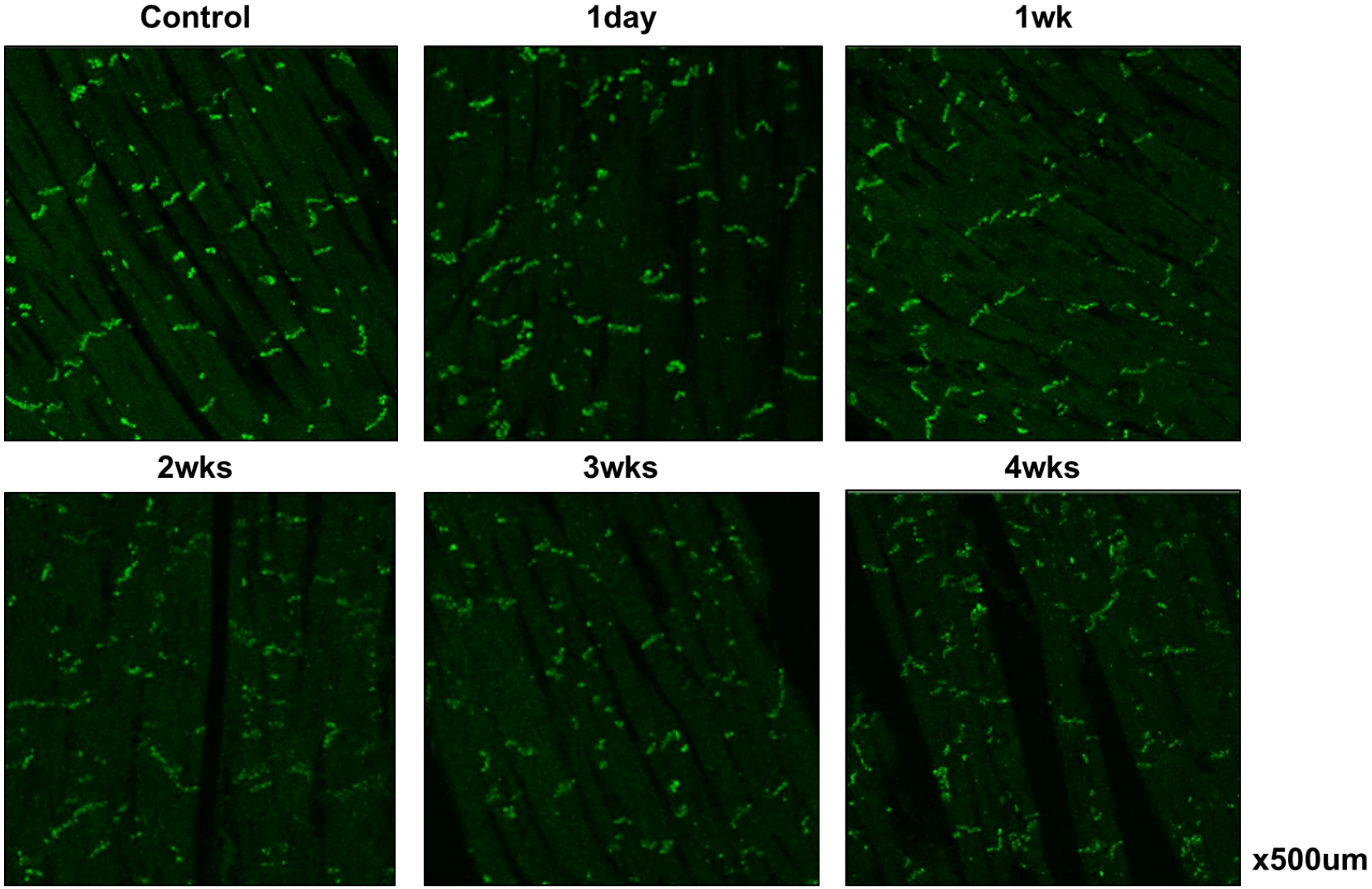

Rat heart, ventricular subendocardium. The connexin-43 expression was decreased at 2 or 3 weeks, but slightly increased at 4 weeks

Figure S3. Positivity of C4d deposition on interstitial vacuolization.

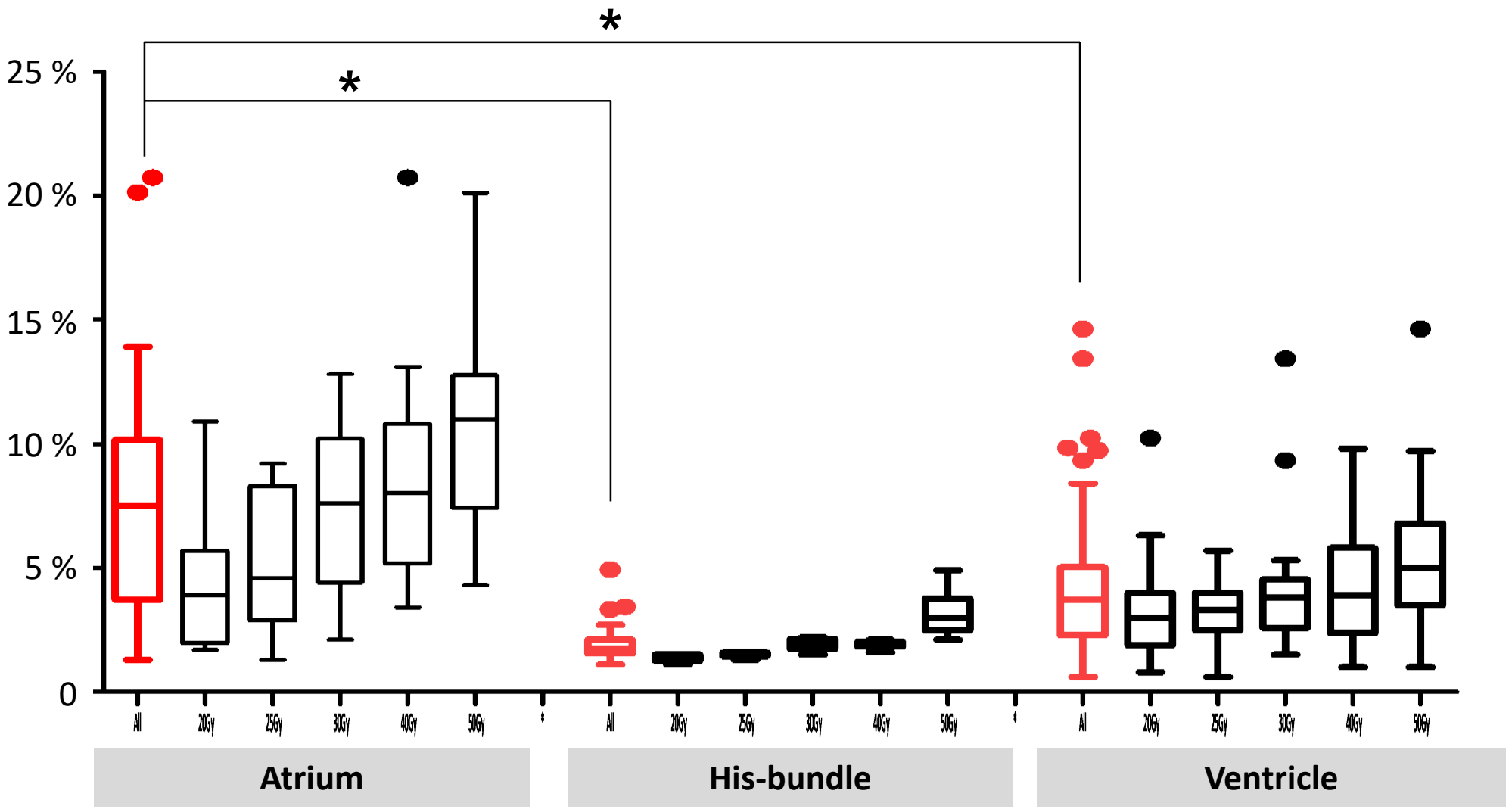

* p <0.05

Figure S4. Immunostaining of capillaries.

	Control	Week 2	Week 4
Capillary distribution	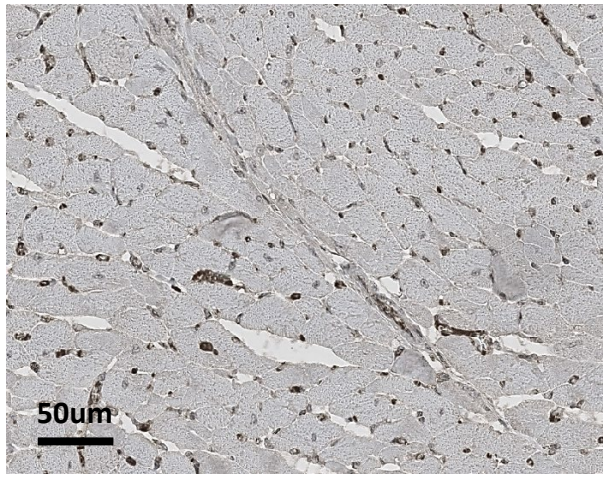	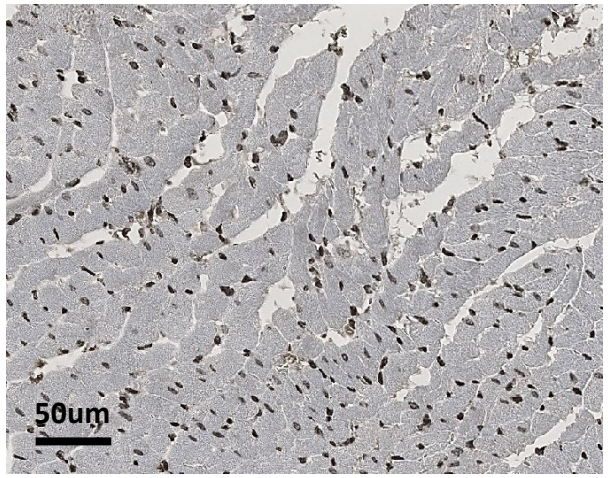	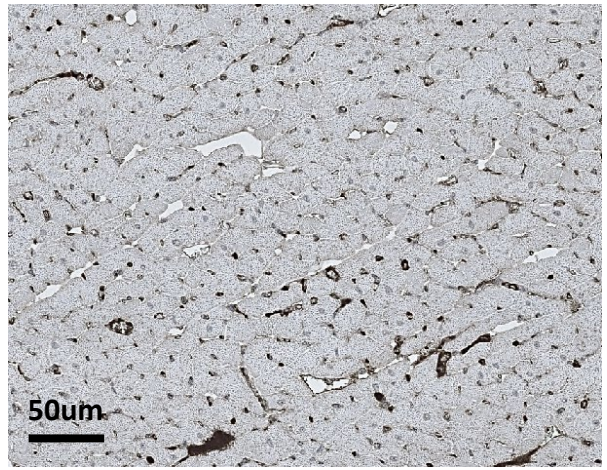
Apoptosis	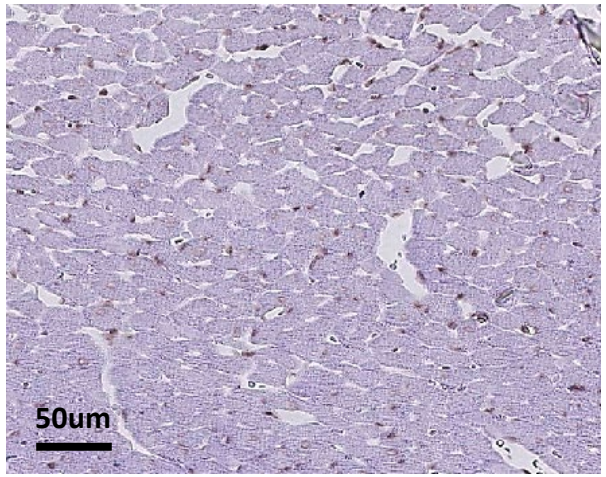	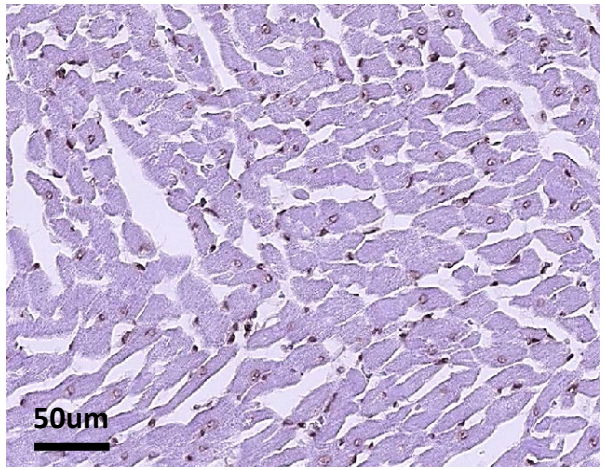	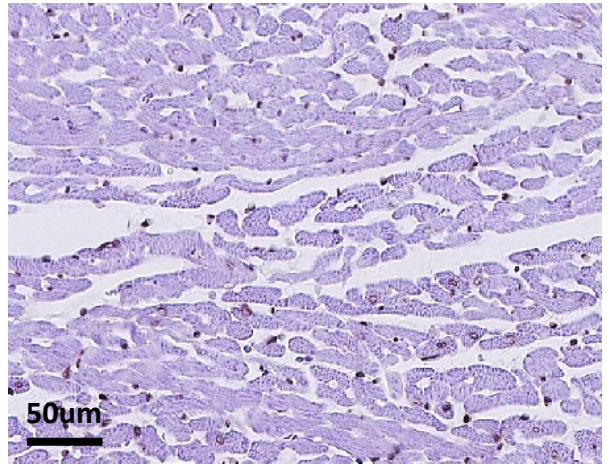

Rat heart, ventricular subendocardium. C4d immunopositivity on vacuolization was less prominent in the His-bundle area than in atrial or ventricular myocardial areas

Figure S5. Intracellular edema with prominent mitochondrial damage.

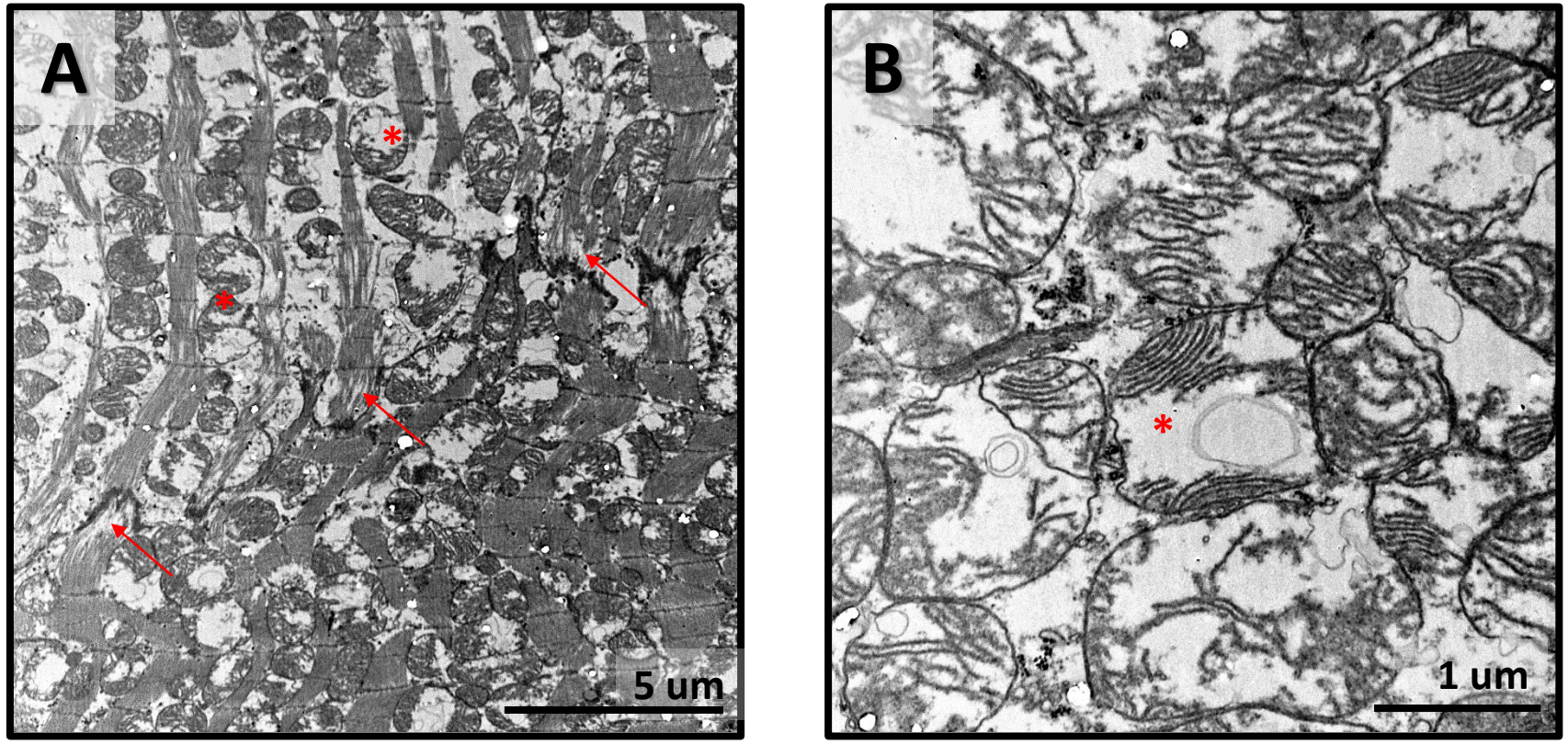

(A) rat heart, ventricular myocardium, electron microscopy (Mag x8000). (B) rat heart, ventricular myocardium, electron microscopy (Mag x30,000), left ventricle irradiated with 30Gy (2 weeks). The inter-myofibrillar widening without discontinuation was marked with red arrows in Panel A. A number of mitochondria were broken and could not maintain their normal shape (Panel B).

Figure S6. Atrium (Left atrial appendage).

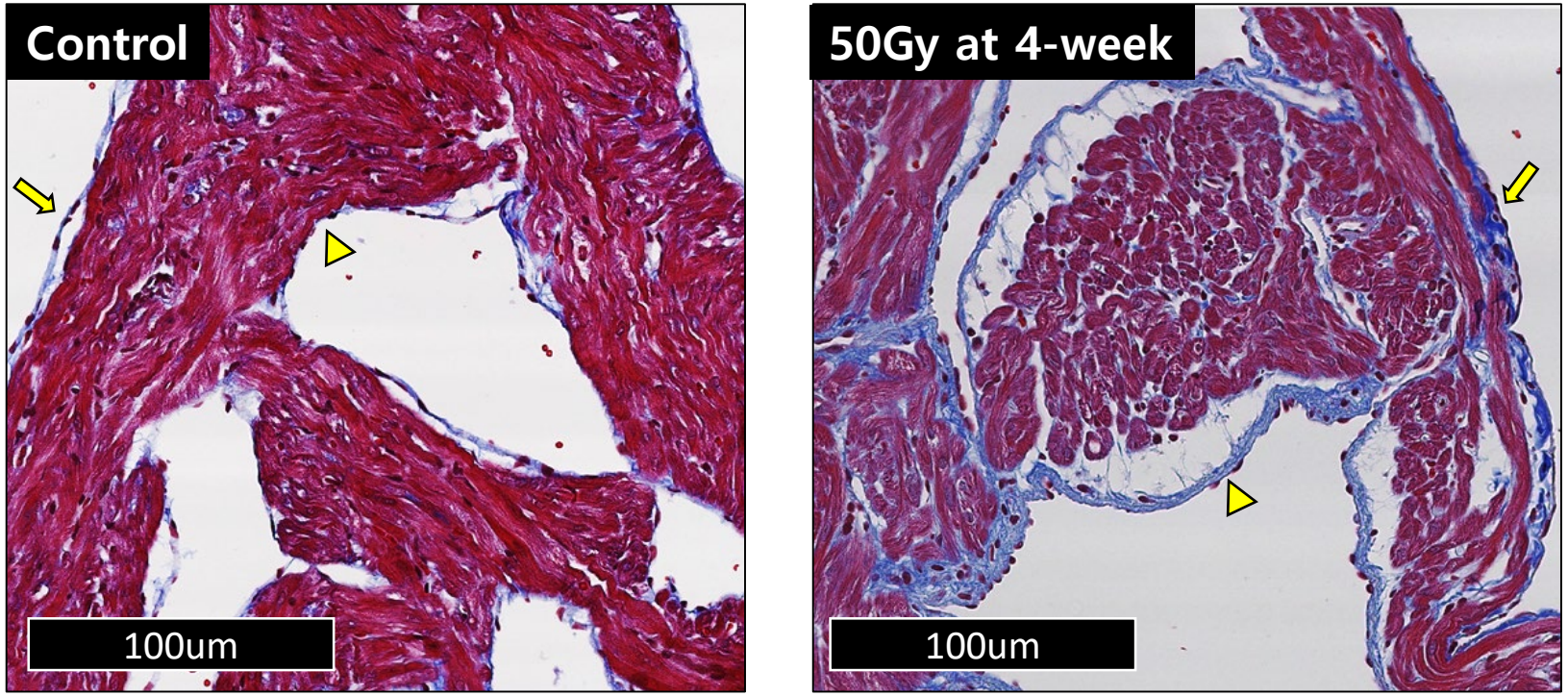

Rat heart, Left atrial appendage (Masson's trichrome staining). Compared to control tissue (left), left atrial appendage (right) irradiated with 50 Gy showed endo-(arrow head) and epi-cardial (arrow) thickening with prominent hyperplasia and interstitial edema. Atrial myocardium also showed myocardial vacuolization most prominent at 3-week and regressed at 4-week. This changes are not definite at 2-week, but at 3-week grossly prominent from 20 to 50 Gy.

Figure S7. Intramyocardial coronary artery.

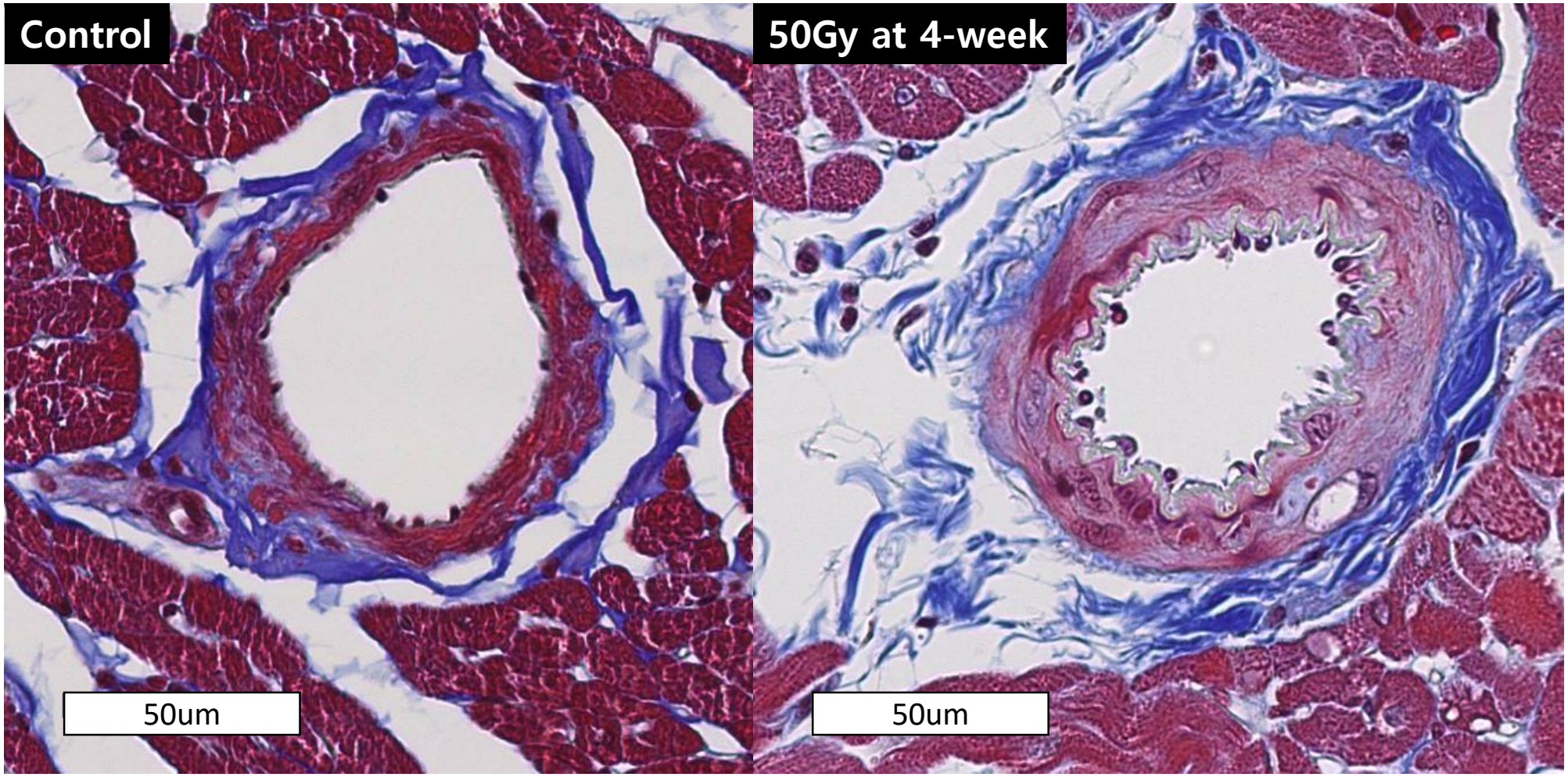

Rat heart, coronary artery. 50Gy/4-week. intimal proliferation and peri-vascular edema starts from 20Gy/2-week with dose/time-dependant manner. Recruitment of fibroblast or inflammatory cells between loosened externa.

Figure S8. Echocardiography.

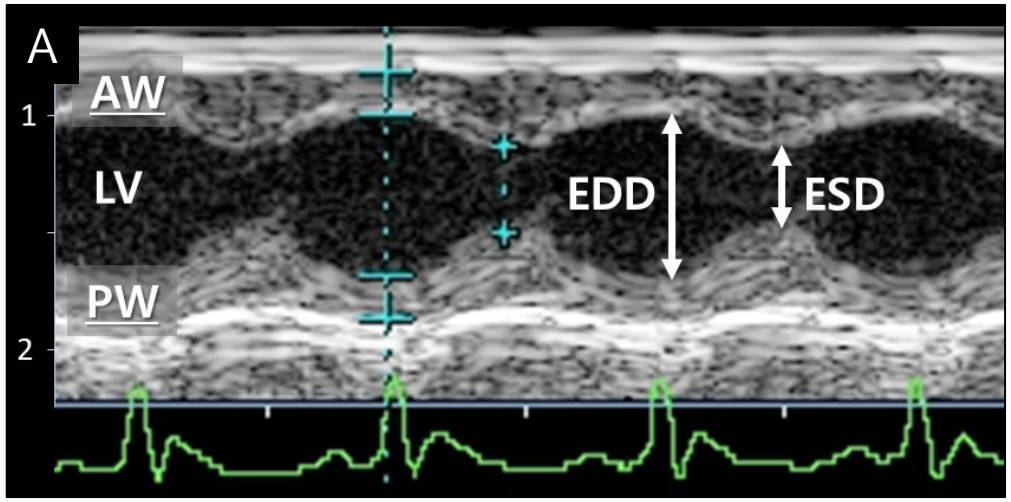

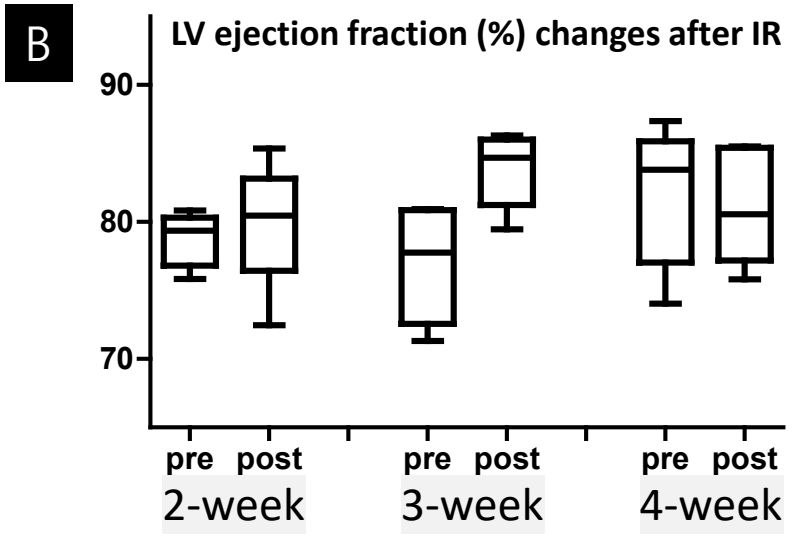

Echocardiographic images or rat heart after 50Gy irradiation. Left ventricular wall thickness and ejection fraction derived by M-mode echocardiography were preserved after irradiation even at 4-week (Panel A). Compared to baseline LVEF (%) before irradiation, there was no statistical significant difference after irradiation at 2-, 3-, and 4-week (Panel B). There was no evidence of wall motion abnormality, valvular dysfunction, pericardial effusion or intracardiac thrombus. LV, left ventricle; AW, anterior wall; PW, posterior wall; EDD, end-diastolic dimension; ESD, end-systolic dimension; LVEF, left ventricular ejection fraction (100xESD/EDD); IR, irradiation

Figure S9. Body weight and laboratory data.

A. Delta body weight (Post IR – Pre IR)

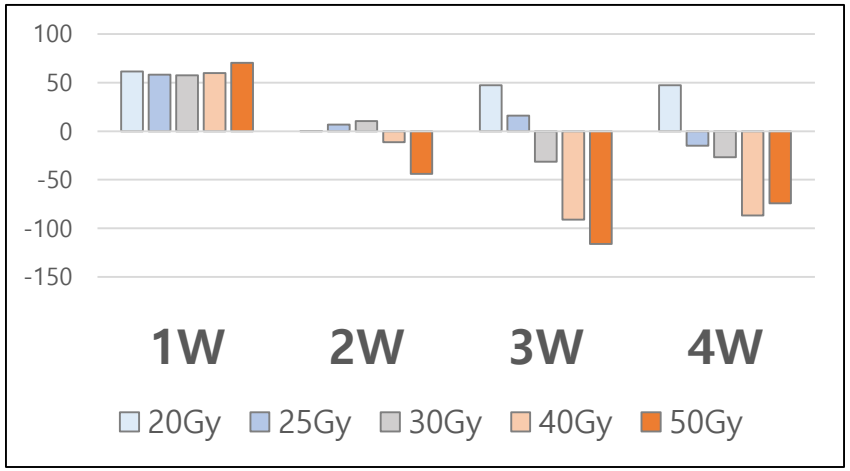

B. Hemoglobin (g/dL)

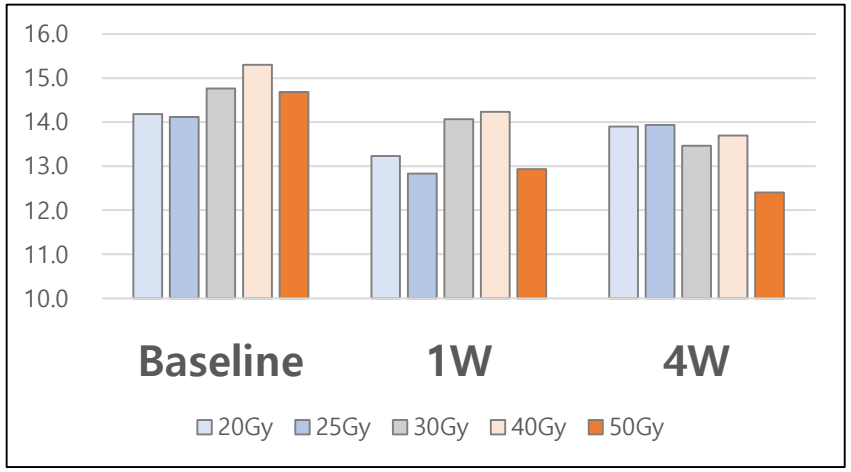

C. White blood cell (×1000/μℓ)

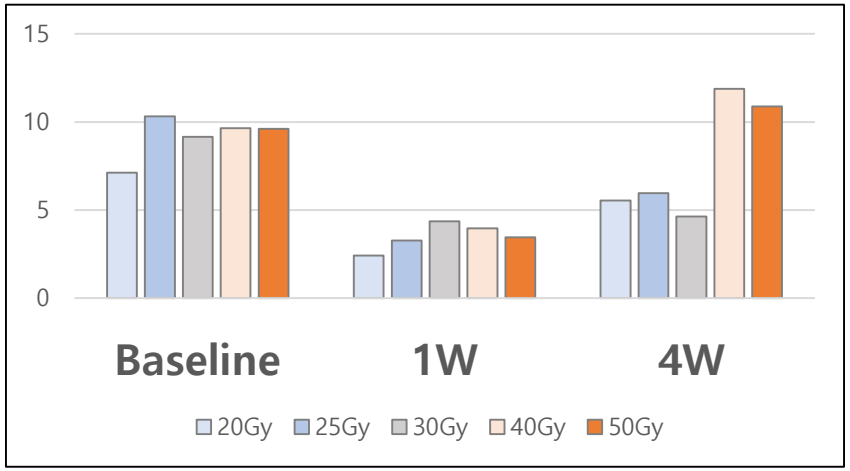

D. The proportion of neutrophil (%)